

# Instant3D: Instant Text-to-3D Generation

Ming Li<sup>1</sup> Pan Zhou<sup>2</sup> Jia-Wei Liu<sup>1</sup> Jussi Keppo<sup>1</sup>  
Min Lin<sup>2</sup> Shuicheng Yan<sup>3</sup> Xiangyu Xu<sup>4\*</sup>

<sup>1</sup>National University of Singapore <sup>2</sup>Sea AI Lab <sup>3</sup>Skywork AI  
<sup>4</sup>Xi'an Jiaotong University

## Abstract

Text-to-3D generation, which aims to synthesize vivid 3D objects from text prompts, has attracted much attention from the computer vision community. While several existing works have achieved impressive results for this task, they mainly rely on a time-consuming optimization paradigm. Specifically, these methods optimize a neural field from scratch for each text prompt, taking approximately one hour or more to generate one object. This heavy and repetitive training cost impedes their practical deployment. In this paper, we propose a novel framework for fast text-to-3D generation, dubbed Instant3D. Once trained, Instant3D is able to create a 3D object for an unseen text prompt in less than one second with a single run of a feedforward network. We achieve this remarkable speed by devising a new network that directly constructs a 3D triplane from a text prompt. The core innovation of our Instant3D lies in our exploration of strategies to effectively inject text conditions into the network. Furthermore, we propose a simple yet effective activation function, the scaled-sigmoid, to replace the original sigmoid function, which speeds up the training convergence by more than ten times. Finally, to address the Janus (multi-head) problem in 3D generation, we propose an adaptive Perp-Neg algorithm that can dynamically adjust its concept negation scales according to the severity of the Janus problem during training, effectively reducing the multi-head effect. Extensive experiments on a wide variety of benchmark datasets demonstrate that the proposed algorithm performs favorably against the state-of-the-art methods both qualitatively and quantitatively, while achieving significantly better efficiency. The project page is at <https://ming1993li.github.io/Instant3DProj/>.

## 1. Introduction

Text-guided 3D content generation has immense potential across diverse applications, such as film production, ani-

\*Project Lead and Corresponding Author.

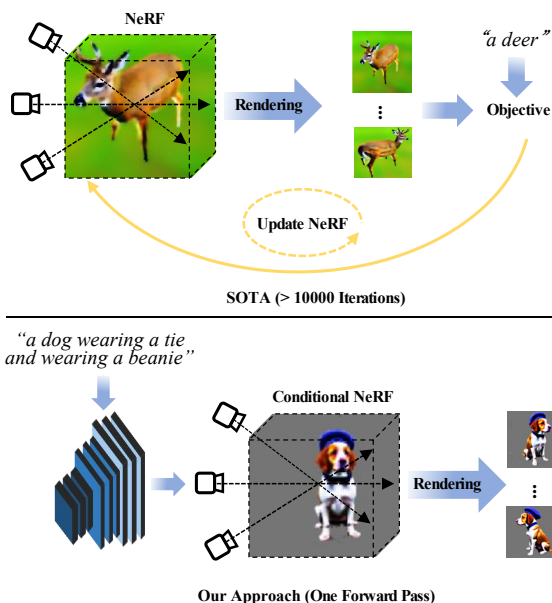


Figure 1: Comparison of existing SOTA methods with our proposal. Existing methods optimize a randomly initialized NeRF from scratch for each text prompt, which usually requires more than 10,000 iterations, taking **hours** to converge. In contrast, our approach is designed to learn a text-conditioned NeRF, which takes much less training computational cost and has strong generalization ability on new prompts. It is able to generate a conditional 3D representation (triplane) of a 3D object for an unseen text prompt in one single pass of a feedforward network, taking about **25ms**.

mation, and virtual reality. Recently, this field has witnessed rapid and notable progress, as exemplified by the pioneering works including DreamFusion [23], Latent-NeRF [18], SJC [9], and ProlificDreamer [43]. These works typically represent a target object with a randomly initialized Neural Radiance Field (NeRF) [19] and then optimize the NeRF under the guidance of 2D diffusion priors leveraging a pre-

trained large-scale text-to-image diffusion model [29].

While achieving impressive results, these works face a critical challenge: they rely on an optimization-based learning paradigm, requiring thousands of iterations to optimize a NeRF for each new input (top of Figure 1). This incurs substantial computational costs and leads to notably slow response speed for practical text-to-3D systems, often taking hours to process a single input [23, 43]. Moreover, since the NeRFs are separately learned for different text inputs, they are not able to leverage general 3D priors shared across objects.

Note that Point-E [22] abandons this optimization paradigm by directly training a diffusion model for 3D point cloud generation. However, these diffusion models require a large number of iterative diffusion steps, which inevitably leads to low efficiency. Besides, it is trained on millions of private 3D assets, which is not feasible for most researchers.

In this paper, we propose a novel framework, named *Instant3D*, for fast text-to-3D generation. It is able to generate a realistic 3D object that faithfully aligns with a given text description, all within a single forward pass of a neural network. Remarkably, this generation process takes less than one second (bottom of Figure 1). The proposed *Instant3D* is a feedforward neural network conditioned on the text prompt and produces a triplane representation [3] encapsulating the desired 3D object. Similar to DreamFusion [23], we use the Score Distillation Sampling (SDS) loss to train our network.

While conceptually simple, this network is substantially challenging to design in practice. The main reason is that the SDS loss provides relatively weak supervision signals, making it difficult to learn an accurate connection between the text condition and the 3D output for a common condition model. This stands in contrast to training models that connect 2D images with texts, such as Stable Diffusion [29] and CLIP [42], where numerous image-text pairs can provide strong supervision signals.

The challenge of weak supervision motivates us to devise more effective condition mechanisms that can better inject text information into the network, alleviating the difficulty of learning the relationship between the two drastically different modalities: text and 3D. As the core innovation of *Instant3D*, our proposed solution to this challenge involves the fusion of three modules: cross-attention, style injection, and token-to-plane transformation. The integration of these components collectively ensures the precise alignment of the generated 3D output with the condition text prompt.

Moreover, we also propose a simple yet effective activation function, called scaled-sigmoid, to replace the original sigmoid function in NeRF, which speeds up the network convergence by more than ten times.

Meanwhile, text-to-3D methods often suffer from severe Janus (multi-head) problems. While the Perp-Neg al-

gorithm [1] can effectively remedy this issue for existing text-to-3D methods, it does not perform well in our context. We find that this is mainly due to the different degrees of multi-head effect exhibited by different 3D objects. As previous text-to-3D approaches only train a single object at a time, one can easily tune the concept negation scale in the Perp-Neg algorithm to adapt to the specific multi-head level. However, in our framework, it is challenging to find a universal, optimum concept negation scale for all various training samples. To tackle this issue, we present an adaptive variant of the Perp-Neg algorithm which dynamically adjusts its concept negation scales according to the severity of the multi-head effect during training, thereby significantly improving the performance.

Our approach demonstrates a powerful capacity to generate a high-quality 3D object consistent with a novel text prompt in only *one second*. We conduct extensive evaluations of the proposed algorithm on a wide variety of benchmark datasets, showing that the *Instant3D* performs favorably against the state-of-the-art approaches both qualitatively and quantitatively with much improved efficiency.

In summary, our contributions are as follows:

- We make early explorations of fast text-to-3D generation with a single run of a feedforward neural network.
- We propose a novel condition model that can effectively absorb text information, facilitating the establishment of the connection between text and 3D under weak supervision.
- We present a new activation function, called scaled-sigmoid, which significantly accelerates the training convergence.
- We present an adaptive Perp-Neg algorithm to better tackle the Janus problem.

## 2. Related Works

**Text-to-Image.** Previously, the research in this field mainly concentrates on generating images belonging to a specific domain or distribution [28, 46, 44, 24, 37, 30]. The literature is dominated by Generative Neural Networks (GANs) [6] and various invariants of GANs are proposed. Recently, inspired by large-scale image-text pairs [34, 33] and generative models, text-to-image generation has shown unprecedented imaginations, *i.e.*, synthesizing all sorts of imaginative images corresponding to text prompts. DALL-E [27] and CogView [4] are developed based on an autoregressive architecture [5, 27], while GLIDE [21] employs a diffusion model [35, 7] conditioned on CLIP guidance [25]. DALL-E-2 [26] also leverages diffusion priors to translate CLIP text embeddings to CLIP image embeddings, followed by synthesizing images from them. Imagen [31] employs a large pre-trained language model to guide the reverse process of a diffusion model in pixel space. It is similar to Stable Diffusion [29]. Differently, the latter is based

on a large-scale UNet architecture and works in the vector-quantized discrete latent space, enabling an efficient sampling process.

**Text-to-3D.** Recent methods of text-to-3D generation without 3D supervision target to generate 3D objects corresponding to input prompts only with the guidance from CLIP or text-to-image models [32, 16, 9, 13, 23, 15, 45].

By leveraging CLIP embeddings to make the generated object closer to the text prompt, DreamFields [9] and CLIP-Mesh [13] trigger the research in this field. They represent 3D objects by NeRFs and spherical meshes, respectively. PureCLIPNeRF [15] follows their paradigm except for replacing NeRFs or spherical meshes with grid-based representation [36]. Inspired by pre-trained large-scale text-to-image diffusion models, DreamFusion [23] proposes a score distillation sampling loss to distill 2D image priors into 3D generation process and achieves much better results than previous works. A concurrent work SJC [41] presents a similar approach. Following this line, Latent-NeRF [18] proposes to learn 3D representations in the latent space instead of pixel space and incorporate more guidance like sketch shapes into the object generation. To solve the problem of low-diversity introduced by SDS, ProlificDreamer [43] presents variational score distillation to construct multiple particles for a single prompt input, sampling the optimal 3D representation from the corresponding probabilistic distribution. These works mainly focus on optimizing an implicit 3D representation for a prompt. Given a new prompt, they need to repeat the optimization process, taking more than one hour. In contrast, our *Instant3D* is able to generate a high-quality 3D object for a new prompt in less than one second after training.

A concurrent work ATT3D [17] follows a similar paradigm to ours, learning a neural network for fast text-to-3D generation. Our *Instant3D* differs from ATT3D in that ATT3D employs a straightforward MLP to learn a hash grid [20], while we devise a novel decoder architecture with enhanced condition mechanisms and a scaled-sigmoid function to generate triplanes, which significantly improves the results. In addition, we present an adaptive Perp-Neg algorithm that effectively tackles the Janus problem. The proposed method achieves higher generation quality and more accurate text-3D alignment than ATT3D, as will be seen later in the experiment P

## 3. Methodology

### 3.1. Preliminaries

#### 3.1.1 Neural Radiance Field

NeRF [19] is an implicit 3D representation widely used in neural inverse rendering. Given a NeRF, rendering an image for a camera view  $c$  involves casting a ray for each pixel of the image; these rays originate from the camera’s center of

projection and extend through the pixel’s location on the image plane, reaching out into the 3D world. Sampled 3D points  $p$  along each ray are then passed through a Multi-Layer Perceptron (MLP), which produces 4 scalar values as output:

$$\begin{aligned}\tau &= f_{\text{softplus}}(f_{\text{MLP}}(p; \theta)[1]), \\ \rho &= f_{\text{sigmoid}}(f_{\text{MLP}}(p; \theta)[2 : 4]),\end{aligned}\tag{1}$$

where  $\tau \in \mathbb{R}$  is volumetric density, indicating the opacity of the scene geometry at the 3D coordinate.  $\rho \in \mathbb{R}^3$  is the albedo, capturing the intrinsic colors that define the scene.  $f_{\text{MLP}}$  represents an MLP with parameters  $\theta$ .  $[i : j]$  denotes extracting channels from  $i$  to  $j$ .  $f_{\text{softplus}}$  is the Soft-plus activation function, ensuring positive volumetric density.  $f_{\text{sigmoid}}$  is the sigmoid function, which confines the albedo to the range of  $[0, 1]$ . These density and albedo values on a ray are then composited with volume rendering, producing the RGB value for the pixel. We use a shading formulation similar to DreamFusion [23] in rendering. Carrying out this process for all pixels on the image plane results in the final rendered RGB image denoted as  $g_\theta(c)$ , which is parameterized by  $\theta$  and conditioned on the camera view  $c$ .

#### 3.1.2 Score Distillation Sampling (SDS)

Most existing text-to-3D methods are based on the SDS loss [23] powered by text-to-image diffusion models [29]. It facilitates the generation of a NeRF from a text prompt by enforcing that the rendered image from the NeRF at any viewpoint maintains semantic consistency with the given text prompt.

In detail, given a rendered image  $g_\theta(c)$ , the SDS loss first introduces random noise  $\epsilon \sim \mathcal{N}(\mathbf{0}, \mathbf{I})$ :

$$\mathbf{x}_t = \sqrt{\alpha_t}g_\theta(c) + \sqrt{1 - \alpha_t}\epsilon,\tag{2}$$

where  $\alpha_{1:T}$  is a predefined decreasing sequence, and the time step  $t$  is selected randomly. Subsequently, a pretrained diffusion UNet  $f_{\text{diffusion}}$  is employed to predict the noise in Equation 2 from  $\mathbf{x}_t$ , which represents the negative score function (NSF) of the image distribution:

$$\begin{aligned}\epsilon_{\text{unc}} &= f_{\text{diffusion}}(\mathbf{x}_t; t), \\ \epsilon_{\text{pos}} &= f_{\text{diffusion}}(\mathbf{x}_t; \mathbf{y}, t) - \epsilon_{\text{unc}}, \\ \epsilon_{\text{predict}} &= \epsilon_{\text{unc}} + w_{\text{guidance}}\epsilon_{\text{pos}},\end{aligned}\tag{3}$$

where  $\epsilon_{\text{unc}}$  is the NSF of the unconditional data distribution, and  $\epsilon_{\text{pos}}$  is the residual NSF conditioned on the text embedding  $\mathbf{y}$ .  $\epsilon_{\text{predict}}$  is based on a classifier-free guidance formulation [8], indicating the direction for updating the image to match the text description  $\mathbf{y}$ , and  $w_{\text{guidance}}$  denotes the guidance weight.

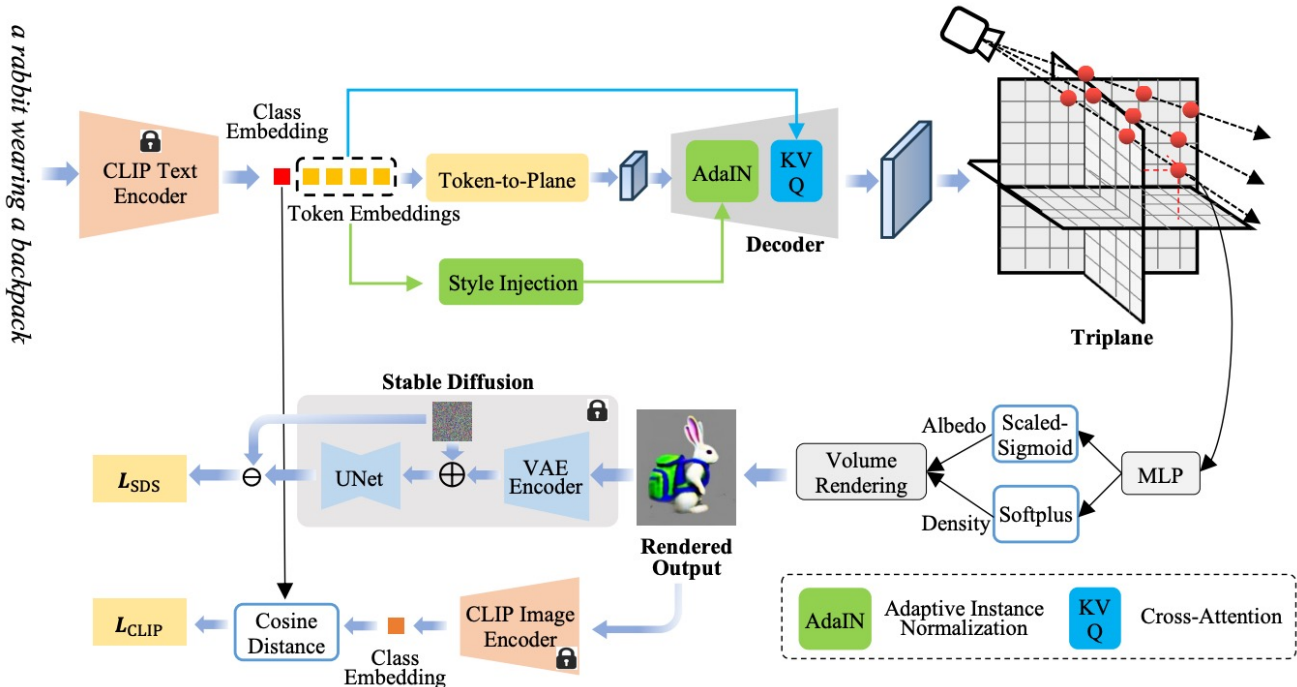


Figure 2: Overview of the proposed *Instant3D*, which applies a conditional decoder network to map a text prompt to a corresponding triplane. Three condition mechanisms, *i.e.*, cross-attention, style injection, and token-to-plane transformation, are seamlessly combined to bridge text and 3D, tackling the issue of weak supervision from SDS [23]. Given a random camera pose, a 2D image is rendered from the conditioned triplane through coordinate-based feature sampling, point density and albedo prediction, and differentiable volume rendering. For albedo activation, we propose a scaled-sigmoid function, effectively accelerating the training convergence. During training, the view image is first diffused by adding random noise and then fed into a pretrained UNet conditioned on the text prompt for denoising, which provides the gradient of the SDS loss. We also present an adaptive Perp-Neg algorithm to better solve the Janus problem in our framework. During inference, our *Instant3D* can infer a faithful 3D object from an unseen text prompt in less than one second.

Finally, the gradient of the SDS loss with respect to the NeRF parameters  $\theta$  can be written as:

$$\nabla_{\theta} \mathcal{L}_{\text{SDS}}(\theta) = \mathbb{E}_{t, \epsilon} \left[ w(t) (\epsilon_{\text{predict}} - \epsilon) \frac{\partial \mathbf{g}_{\theta}(c)}{\partial \theta} \right], \quad (4)$$

where  $w(t)$  is a weight function depending on  $\alpha_t$ .

### 3.2. Conditional NeRF Generation

By combining NeRF and SDS, existing methods [23, 18, 40] have demonstrated impressive results for text-to-3D generation. However, these methods suffer from an important drawback that they need to train a new NeRF for each new text prompt, leading to low efficiency. To address this issue, we propose to learn a single feedforward network *Instant3D* for multiple text prompts, enabling fast text-to-3D generation. An overview of *Instant3D* is shown in Figure 2.

In particular, we design a conditional network  $f_{\text{Instant}}(p, \mathbf{y}; \theta)$ , which is conditioned on the text feature  $\mathbf{y}$ . We obtain the text feature with the pretrained text

encoder of CLIP [42]. The conditional network can be formulated as:

$$f_{\text{Instant}}(p, \mathbf{y}; \theta) = \hat{f}_{\text{MLP}}(f_{\text{sam}}(p, f_{\text{dec}}(\mathbf{y}; \theta_1)); \theta_2). \quad (5)$$

Inspired by StyleGAN [11], we adopt a decoder architecture  $f_{\text{dec}}$  to transform the text condition  $\mathbf{y}$  into a triplane [3]. Then we sample a feature vector for each 3D point  $p$  from the triplane using  $f_{\text{sam}}$ , which projects  $p$  onto each plane, retrieves the corresponding feature vector via bilinear interpolation, and aggregates the three feature vectors via concatenation [3]. This point feature is subsequently sent to an MLP  $\hat{f}_{\text{MLP}}$  to produce the density and albedo values. The parameters of the conditional model  $\theta$  include both the decoder parameters  $\theta_1$  and MLP parameters  $\theta_2$ . Replacing  $\hat{f}_{\text{MLP}}$  with  $f_{\text{Instant}}$  in Equation 1 enables conditional NeRF prediction, where different  $\mathbf{y}$  yields different NeRF outputs, and the learned model parameters  $\theta$  are shared among diverse text prompts.

The key component in Equation 5 is the decoder network which plays the role of transferring text information into

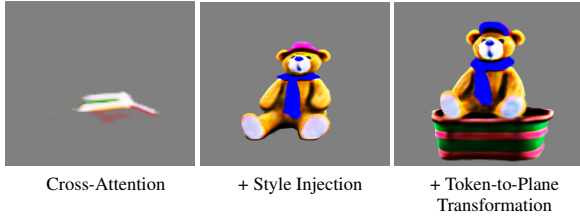


Figure 3: Integrating three condition mechanisms produces high-quality results faithful to the text prompt. The prompt here is “a teddy bear sitting in a basket and wearing a scarf and wearing a baseball cap”.

3D. While conceptually simple, designing such a decoder in our framework poses substantial challenges. The main reason is that the SDS loss in Equation 4 provides relatively weak supervision signals, which impedes learning a robust connection between the text condition and the 3D output. This is in contrast to text-to-image models, such as Stable Diffusion [29] and CLIP [42], where numerous image-text pairs can provide strong supervision signals.

The weak supervision issue demands a more effective conditional model that can better absorb text information, alleviating the difficulty of bridging text and 3D. To this end, we introduce an integrated solution combining three condition mechanisms: cross-attention, style injection, and token-to-plane transformation.

### 3.2.1 Cross-Attention

Cross-attention is one of the most important strategies for information interaction across various modalities. Following the prominent success of text-to-image models, we apply cross-attention to inject text descriptions into the 3D representation. Similar to Stable Diffusion [29], we employ the multi-head cross-attention module (MHCA) to fuse text embeddings with feature maps of the decoder, where the Query is the feature maps, and the Key and Value are projected text features.

### 3.2.2 Style Injection

Surprisingly, the model with only the cross-attention mechanism completely fails, yielding a meaningless output as shown in Figure 3. Upon closer inspection, we find this is mainly due to that a single text input can be associated with multiple plausible 3D objects. However, the cross-attention is inherently deterministic and cannot capture this ambiguity. To address this issue, we introduce the Adaptive Instance Normalization (AdaIN) to inject random noise (known as “style” in StyleGAN [11]) into the decoder.

Different from StyleGAN, we also encode text features into the style by introducing a style injection module to im-

prove the controllability of the 3D generation process. As shown in Figure 4, the style injection module starts with a linear projection layer to more compactly represent the text embeddings. Subsequently, we apply a self-attention module to adapt the feature to the style space. The output text features are flattened to a vector and concatenated together with random Gaussian noise to generate the style vector. Finally, the output vector of the style injection module is embedded into the feature maps of our decoder network with AdaIN in Figure 2.

### 3.2.3 Token-to-Plane Transformation

Existing decoder architectures typically start with a learnable planar base tensor [11, 12, 10], which is kept constant after training. In contrast, we reformulate this paradigm by predicting the base tensor from the text embedding with a token-to-plane transformation module as shown in Figure 2. Consequently, the base tensor evolves from a static entity to a dynamic one, significantly deviating from the common practices of StyleGAN, which can better convey condition information to the decoder.

As illustrated in Figure 5, we employ a self-attention module to transform sequential token embeddings into a 2D feature map. Specifically, we first reduce the dimension of tokens with linear projection for more efficient computations. Then a multi-head self-attention (MHSA) layer [39] is performed to enable global information interaction among tokens. We further apply an MLP to refine the token embeddings and then reshape them to a feature map with the shape of  $8 \times 8$ . The token-to-plane transformation not only transforms the sequential tokens into a desired planar shape, but also shifts the CLIP embeddings to a feature space suitable for text-to-3D generation.

As shown in Figure 3, the integration of all three condition mechanisms collectively ensures the precise alignment of the generated 3D output with the condition text prompt.

**Text Feature.** The text encoder of CLIP [25] generates both class and token embeddings for a text prompt. The class embedding usually contains sentence-level semantic information. In contrast, the token embeddings contain rich word-level semantic details of a prompt, which can better represent items in a scene and are commonly used in text-to-image generation [29]. We aim for the generated 3D objects to reflect all mentioned entities and maintain their inherent relationships, matching the token-level granularity of the text prompt. Thus, we use the token embeddings as the text feature to guide our 3D generation, which leads to superior generation results on novel prompts.

### 3.3. Scaled-Sigmoid

As shown in Equation 1, the sigmoid function is usually used to ensure the albedo prediction falls within the range

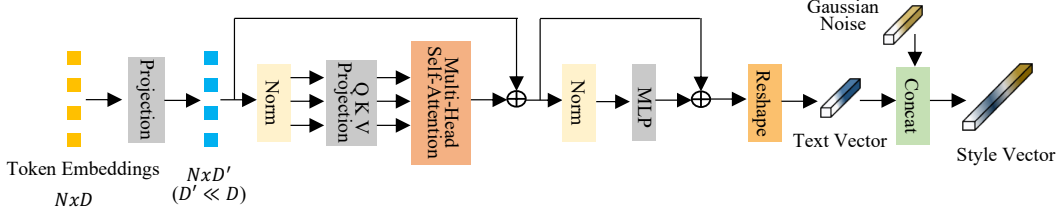


Figure 4: Illustration of our style injection module, which takes token embeddings extracted by the CLIP text encoder as input while incorporating Gaussian noise into the generative style vector.

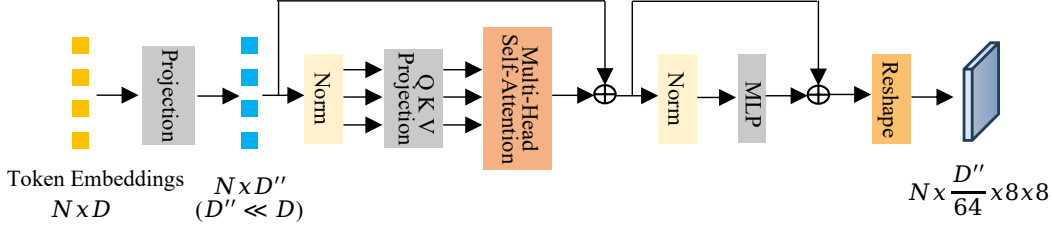


Figure 5: Illustration of our token-to-plane transformation, which starts with token embeddings extracted by the CLIP text encoder and outputs a 2D feature map with the shape of  $8 \times 8$ . A multi-head self-attention layer dominates the transformation and enables global information interaction between token embeddings.

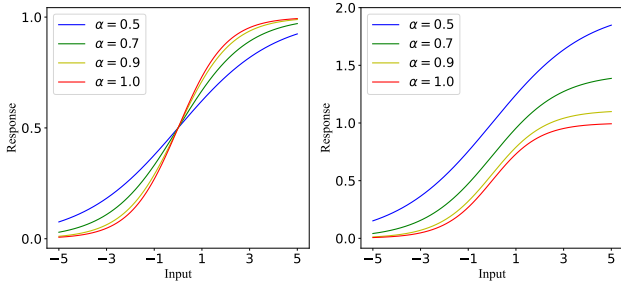


Figure 6: Comparison of the original sigmoid function with its stretched variant (left) and the proposed scaled-sigmoid function (right). With  $\alpha < 1.0$ , the scaled-sigmoid function possesses a broader high-gradient region, which accelerates training.

of  $[0, 1]$ . However, we observe that applying the conventional sigmoid to albedo causes difficulties in training convergence. A deeper analysis reveals that the MLP output may exceed the high-gradient region around zero, leading to gradient vanishing. This phenomenon significantly impedes the learning of the 3D representation, resulting in extended training durations and occasional convergence failures.

To address this issue, we stretch the high-gradient region by multiplying the input with a fractional coefficient  $\alpha$ :

$$\hat{f}_{\text{sigmoid}}(x) = f_{\text{sigmoid}}(\alpha x), \quad \alpha \in [0, 1]. \quad (6)$$

The behavior of  $\hat{f}_{\text{sigmoid}}$  with different  $\alpha$  is shown in Figure 6 (left). Note that the stretching operation reduces the gradient by a factor of  $\alpha$ . To counter this effect, we further

apply a scaling factor of  $\frac{1}{\alpha}$  to the stretched sigmoid:

$$\tilde{f}_{\text{sigmoid}}(x) = \frac{1}{\alpha} f_{\text{sigmoid}}(\alpha x), \quad \alpha \in [0, 1]. \quad (7)$$

We refer to  $\tilde{f}_{\text{sigmoid}}$  as the scaled-sigmoid, which is visualized in Figure 6 (right). Since  $\tilde{f}_{\text{sigmoid}}$  can surpass the  $[0, 1]$  bounds, we employ an annealing strategy: initializing  $\alpha$  with a small value (0.5 in our experiment) to accelerate training; over time, we gradually increase  $\alpha$  to 1, ensuring the output albedo lies in  $[0, 1]$ .

### 3.4. Adaptive Perp-Neg Algorithm

**Previous Perp-Neg Algorithm.** Existing text-to-3D algorithms often face a challenging Janus (multi-head) problem [18]. Rather than generating a coherent 3D output, the learned 3D object tends to exhibit repeated front views at different angles, as the front view has been more prominent in the training data of text-to-image models. For instance, when generating a 3D animal, the resulting output often has multiple faces without capturing the natural side and back views of the animal.

To address this issue, [1] propose a Perp-Neg algorithm:

$$\begin{aligned} \epsilon_{\text{predict}} &= \epsilon_{\text{unc}} + w_{\text{guidance}} (\epsilon_{\text{pos}} - w_{\text{neg}} \epsilon_{\text{neg}}^{\perp}), \\ \epsilon_{\text{neg}} &= f_{\text{diffusion}}(\mathbf{x}_t; \mathbf{y}_{\text{neg}}, t) - \epsilon_{\text{unc}}, \end{aligned} \quad (8)$$

where  $\epsilon_{\text{predict}}$  is used in Equation 4 to calculate the gradient of the SDS loss.  $\mathbf{y}_{\text{neg}}$  denotes the token embeddings of negative prompts. For example, when rendering images at

the back view, the negative prompts refer to side and front views.  $\epsilon_{\text{neg}}$  is the residual NSF of negative text prompts, penalizing the generation of wrong views at inappropriate angles.  $\perp$  indicates projection onto the direction perpendicular to  $\epsilon_{\text{pos}}$ .  $w_{\text{neg}}$  represents the concept negation scale, controlling the degree to which Equation 8 penalizes the Janus problem.

**Adaptive Adjustment.** Selecting an appropriate value for  $w_{\text{neg}}$  is critical for the success of Perp-Neg. If it is too small, the Janus effect will not be sufficiently mitigated. If it is too large, it may cause the flat-head issue, where the entire head is squeezed into a flat plane. This is because the  $y_{\text{neg}}$  in Equation 8 punishes front views when rendering in side angles, and a flat head ensures no face can be seen from a side perspective. For existing optimization-based methods, it is feasible to manually adjust  $w_{\text{neg}}$  for each new text prompt. However, as our model is trained on an extensive set of text prompts, it is challenging to find a universally optimum concept negation scale for all training samples. To overcome this challenge, we propose an adaptive Perp-Neg algorithm to dynamically adjust the value of  $w_{\text{neg}}$  according to the severity of the multi-head problem for different samples.

Specifically, we design the negation scale in our adaptive Perp-Neg as

$$w_{\text{neg}} = w_{\text{min}} + C \cdot \Delta w, \quad (9)$$

where  $w_{\text{min}}$  is the minimum scale, and  $\Delta w$  describes the variation range of  $w_{\text{neg}}$ . The adaptive parameter  $C \in [0, 1]$  measures the severity of the multi-head problem. When the multi-head effect is less pronounced ( $C = 0$ ), we apply a small punishment in Equation 8 with  $w_{\text{neg}} = w_{\text{min}}$ . Conversely, when the multi-head effect is highly severe ( $C = 1$ ), the negation scale increases to  $w_{\text{min}} + \Delta w$ .

To assess the severity of the multi-head problem for a given rendered image  $I_v$  at the current viewpoint  $v$ , we define  $C$  as:

$$C = \frac{1}{4n} \sum_{i=1}^n [1 - \cos(v - v_i)] \cdot [1 + \langle \phi(I_v), \phi(I_{v_i}) \rangle], \quad (10)$$

where we randomly select  $n$  additional views  $\{v_i\}_{i=1}^n$  and measure the similarity between  $I_v$  and each  $I_{v_i}$  in feature space. The feature extractor  $\phi$  is the image encoder of CLIP [42], and  $\langle \cdot, \cdot \rangle$  represents the cosine similarity. The rationale for this design is that a higher similarity between different views indicates more severe multi-head effect, and conversely, a lower similarity value among different views suggests a less significant Janus problem. Besides, we weight the contribution of different view angles in Equation 10 with  $1 - \cos(v - v_i)$ . This weighting mechanism takes into account that high similarity between views that are farther apart indicates a more severe multi-head effect.

While Equation 10 offers an effective approach for adjusting the negation scale adaptively, it comes with a notable computational overhead. This is primarily due to the extra cost involved in rendering  $\{I_{v_i}\}_{i=1}^n$ . To address this issue, we adopt a simplified approach by setting  $n = 1$  and utilizing the rendered image from the previous iteration as the additional view. To facilitate this process, we maintain a cache that stores image features  $\phi(I_v)$  for all training samples. This cache enables us to reuse the feature representations extracted during the preceding training steps. The features in the cache are dynamically updated, where the current feature is added while the old feature is removed. This approach allows us to implement adaptive Perp-Neg without introducing additional computational costs.

### 3.5. Training Objective

Except for the SDS loss in Section 3.1.2, the proposed *Instant3D* also incorporates a CLIP loss  $\mathcal{L}_{\text{CLIP}}$ . As shown in Figure 2, we employ the CLIP image encoder to extract image features from the rendered image and use the class embeddings from the CLIP text encoder to represent the text prompt. We then define the CLIP loss as the cosine distance between the image and text features to align the rendered image more closely with the input prompt. Remarkably, these two training objectives allow learning a text-to-3D model without requiring any 3D data.

## 4. Experiments

### 4.1. Datasets

As this work is a pioneering effort for fast text-to-3D generation, we devise three benchmark prompt sets to comprehensively evaluate the proposed framework: Animals, Portraits, and Daily Life.

**Animals.** This prompt set is constructed by combining several keywords, where each keyword can be randomly chosen from a predefined set of candidates:

- **species:** *wolf, dog, panda, fox, civet, cat, red panda, teddy bear, rabbit, and koala.*
- **item:** *in a bathtub, on a stone, on books, on a table, on the lawn, in a basket, and null.*
- **gadget:** *a tie, a cape, sunglasses, a scarf and null.*
- **hat:** *beret, beanie, cowboy hat, straw hat, baseball cap, tophat, party hat, sombrero, and null.*

A sample prompt is structured as “a **species** sitting **item** and wearing **gadget** and wearing a **hat**”. The *null* means the keyword is absent from the prompt. In total, the Animals set consists of 3,150 prompts. We randomly allocate 60% of them for training and the remaining 40% for testing.

**Portraits.** We construct this prompt set by describing portraits of commonly seen figures with various hats and facial expressions. The keywords and their available choices include:

- **figure:** *a white man, a white woman, a boy, a girl, an elderly man, an elderly woman, a black woman, a black man, Obama, Kobe.*
- **hat:** *Santa hat, peaked cap, steampunk hat, crown.*
- **expressing:** *laughing, crying, grinning, singing, shouting, looking ahead with a very serious expression, opening mouth wide in shock, angry, talking, feeling sad.*

These keywords are combined in the manner of “**figure** wearing a **hat** is **expressing**”. The Portraits set consists of 400 prompts in total, with 60% for training and 40% for testing.

**Daily Life.** The above two prompt sets are constructed by combining phrases from a limited range of candidates in a structured manner. To demonstrate that our approach can work well in a more general setting where more complex and varied sentences are included, we contribute another dataset named Daily Life by collaborating with ChatGPT [2]. ChatGPT is a large language model designed to converse with humans and can produce high-quality responses when given appropriate context. We craft our question as “*generate a text describing a man or woman’s appearance and daily activities. The examples are as follows: a tall man wearing sunglasses is eating a hamburger, a slim woman wearing a baseball cap is reading a book, a beautiful woman wearing a tie is watching a TV*”. By repeatedly submitting this question to ChatGPT, we collect more than 17,000 answers as our prompt set. These prompts exhibit a wide variety of structures and contain 3,135 unique words in total, demonstrating enhanced complexity and diversity. We train our framework on the whole set and perform evaluation by generating additional new prompts via ChatGPT.

## 4.2. Implementation Details

**Camera Setting.** For NeRF rendering, we randomly sample a camera pose in a spherical coordinate system with the polar angle  $\gamma \in [25^\circ, 110^\circ]$ , azimuth angle  $\phi \in [0^\circ, 360^\circ]$ , and radius from the origin  $r \in [3.0, 3.6]$ . The camera FOV is randomly selected between  $70^\circ$  and  $80^\circ$ .

**Neural Rendering.** For volumetric rendering, 128 points are sampled along each ray. Among them, 64 points are uniformly sampled, and the remaining 64 are sampled based on the importance distribution along the ray. The resolution of rendered images is  $64 \times 64$  during training and increased to  $256 \times 256$  for testing.

**Architecture.** Our decoder network is composed of attention blocks and convolution blocks similar to Stable Diffusion [29]. More details can be found in the appendix.

**Optimization.** We use the Adam optimizer [14] with a learning rate of  $1e-4$ ,  $\beta_1 = 0.9$ ,  $\beta_2 = 0.99$  and a zero weight decay. All experiments are conducted on NVIDIA A100 GPUs. Training on Animals and Daily Life prompt sets is performed on 8 GPUs with a batch size of 96, which

takes about 8 hours and 60 hours, respectively. Training on Portraits uses 4 GPUs with a batch size of 48, taking about 3.5 hours. For inference, given a new text prompt, the generation of the 3D triplane takes about 25ms, and the rendering of one view image at a resolution of  $256 \times 256$  takes about 0.5s.

## 4.3. Comparison with the State-of-the-Art Methods

**Qualitative Comparison.** We compare with the state-of-the-art text-to-3D methods including TextMesh [38], SJC [41], DreamFusion [23], Latent-NeRF [18] and Prolific-Dreamer [43] (implemented by ThreeStudio<sup>1</sup>). Note that these methods typically take more than an hour to optimize a NeRF for an input prompt, while our framework can generate a 3D object in under a second.

Meanwhile, since our model is trained on a large set of text inputs, it is able to leverage general 3D priors shared across objects. Therefore, the generated objects by *Instant3D* have much higher quality than the baselines as illustrated in Figure 7 and 8. Besides, our method captures all elements specified in the prompts as well as the relationships between them. In contrast, objects produced by the baseline approaches frequently miss important items, and their inter-item relationships can appear disorganized.

In addition, we provide a comparison with Point-E [22], which directly trains a 3D diffusion model. This method is based on a substantially different paradigm and requires millions of 3D-text pairs that are not available to the public. In contrast, our algorithm does not require any 3D data. Moreover, due to the limitation of the 3D datasets, especially in terms of scale and diversity, Point-E can only generate simple objects and cannot perform well on more intricate text prompts as shown in Figure 7.

Finally, we present more visual examples from the Animals, Portraits, and Daily Life datasets in Figure 9-11. The proposed *Instant3D* consistently produces high-quality text-to-3D results with favorable multi-view consistency. Notably, its performance on the challenging Daily Life dataset (Figure 11) underscores its capability to handle intricate real-world text prompts.

**Computation Costs.** To evaluate the training costs of different methods, we report the number of rendered view images per prompt on average (Views-PP) vs. CLIP retrieval probability (CLIP-RP) on the Animals set. Views-PP is computed as:

$$\text{Views-PP} = \frac{\text{Iterations} \times \text{Batch Size}}{\text{Number of Prompts}}, \quad (11)$$

which essentially measures the computation cost as the number of images rendered for each prompt during training. CLIP-RP is defined as the average probability of assigning the correct prompt to a rendered image among a

<sup>1</sup><https://github.com/threestudio-project/threestudio>

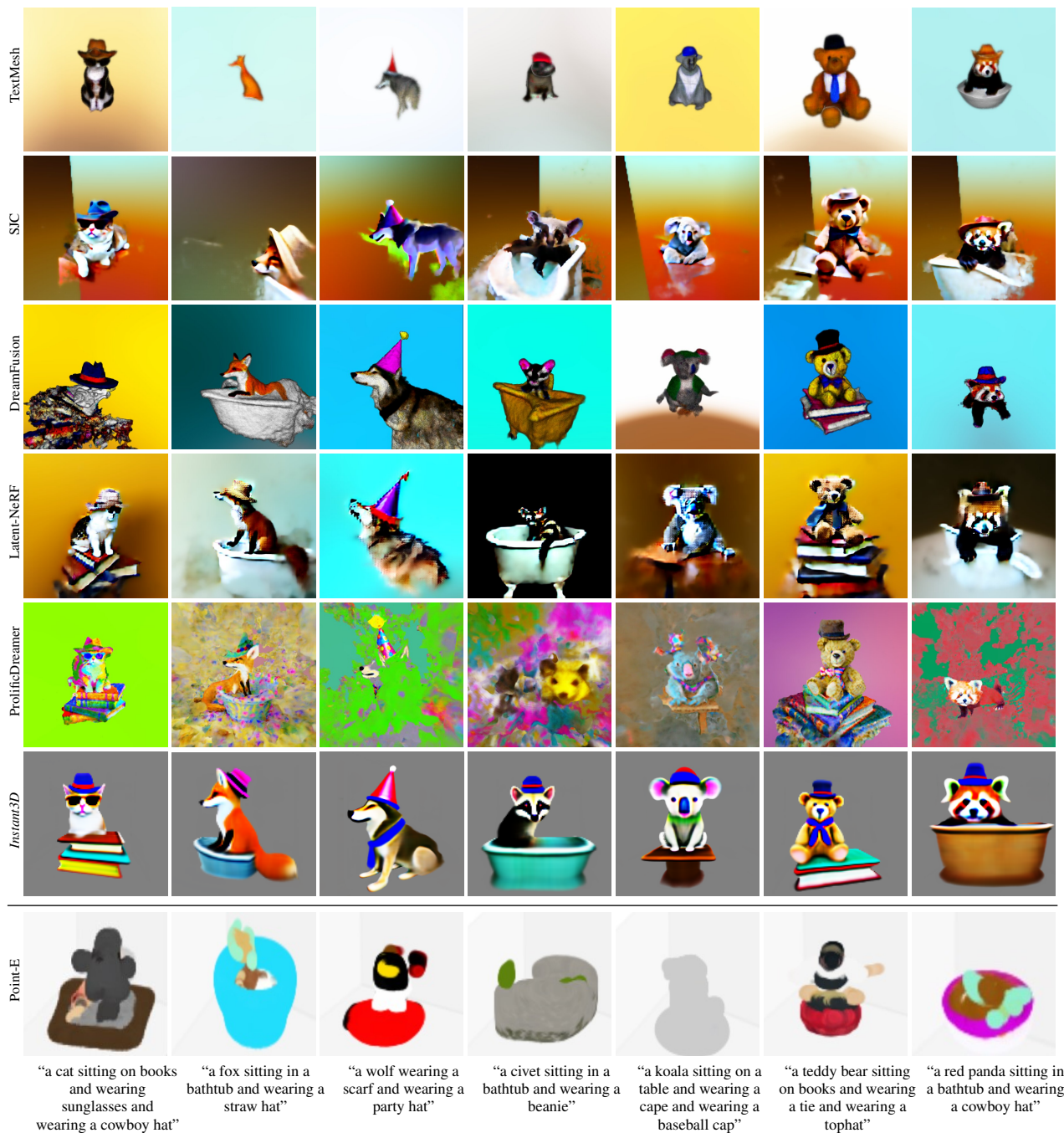


Figure 7: Qualitative comparison with the state-of-the-art methods including TextMesh [38], SJC [41], DreamFusion [23], Latent-NeRF [18], ProlificDreamer [43], and Point-E [22] on the Animals dataset. The proposed *Instant3D* achieves higher-quality results while being much more efficient than the baselines.

set of distraction texts (called the query set). The similarity between a text and an image is measured by CLIP text and image encoders. For each prompt, the CLIP-RP is averaged over four view images rendered from distinct camera poses as in DreamFusion [23]. All prompts of the Animals

set are used as the query set. As shown in Figure 12, the generation quality generally gets better as the training iteration increases, while the improvement speed of the baseline methods is much slower than that of our *Instant3D*. Notably, the baselines can only achieve an acceptable CLIP-RP after

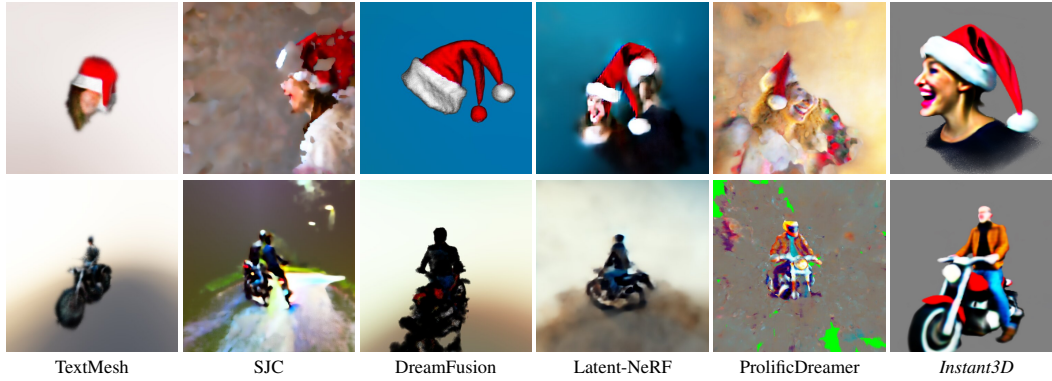


Figure 8: Qualitative comparison against the baseline approaches on the Portraits (top) and Daily Life (bottom) datasets. The prompts for the top and bottom are “woman” and “a handsome man wearing a leather jacket is riding a motorcycle”, respectively.

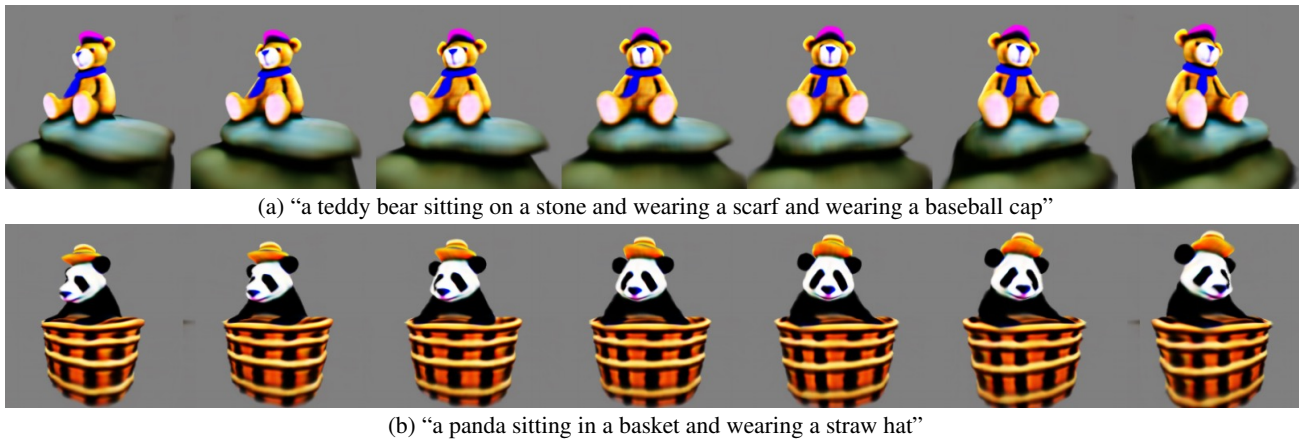


Figure 9: Visual results on the Animals set, which are inferred by our *Instant3D* for novel prompts. The results demonstrate accurate text-3D alignment and satisfying multi-view consistency.

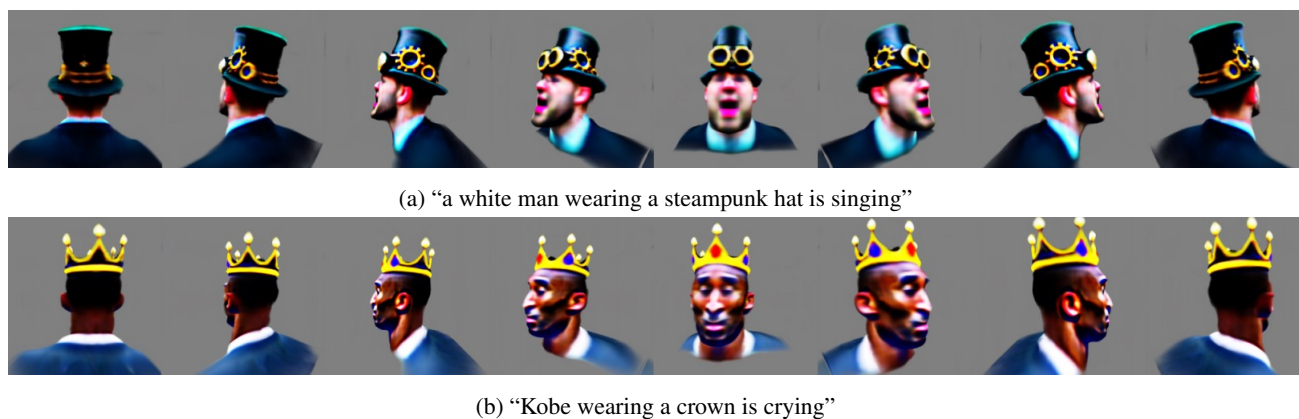


Figure 10: Visual results on the Portraits set. Our *Instant3D* accurately generates the figures, items, and expressions described in the text prompts, while showing favorable multi-view consistency.

10,000 iterations per prompt. In contrast, our method obtains a much higher CLIP-RP score in only 2,000 iterations per prompt.

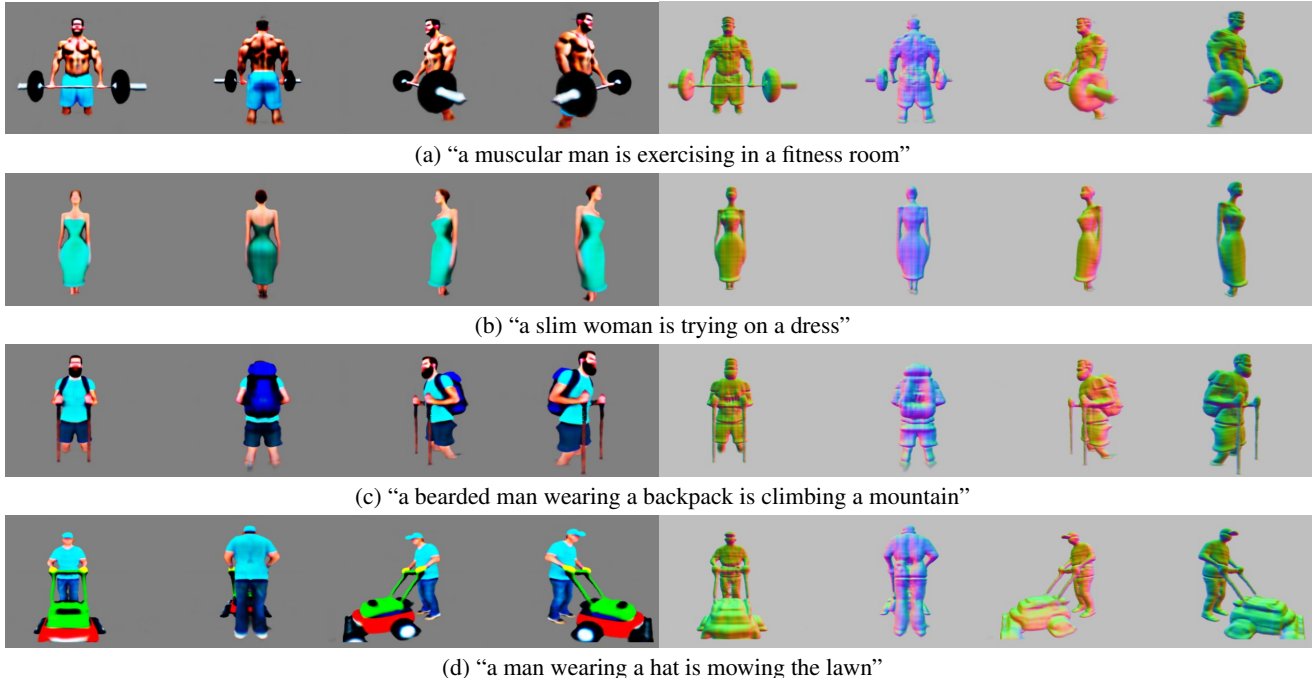


Figure 11: Visual results on the Daily Life set. For each prompt, four views and their normal images are shown, demonstrating that our *Instant3D* is able to generate complex and diverse objects with accurate geometric details for novel prompts.

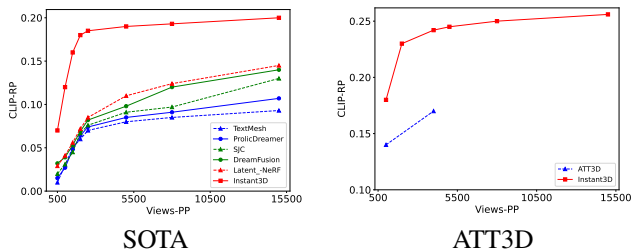


Figure 12: Computation cost comparison against the baseline methods. Left: comparison with the state-of-the-art methods on the Animals dataset. Right: comparison with a concurrent approach ATT3D on their dataset. Views-PP is the number of rendered images per prompt in training, and CLIP-RP is the retrieval probability computed by CLIP encoders.

Table 1: User study for comparing our method with the baseline approaches in terms of realism and text-3D consistency.

Method	TextMesh	SJC	DreamFusion	Latent-NeRF	ProlificDreamer	<i>Instant3D</i>
Realism	4.22%	4.95%	6.32%	7.49%	1.74%	75.28%
Consistency	2.35%	3.91%	3.69%	5.10%	1.33%	83.62%

**User Preference Study.** We conduct a user study to evalu-

ate different methods based on subjective perceptual quality assessment. We show users videos rendered from multiple views of objects, generated by different methods using the same text prompt. Users are asked to select the result that most closely matches the description in terms of realism and consistency. Each prompt is evaluated by at least 3 different users. As shown in Table 1, most users prefer our results to those generated by baselines, highlighting the effectiveness of *Instant3D* in achieving high fidelity and accurate text-3D alignment.

#### 4.4. Comparison with ATT3D

In this section, we compare our method with a concurrent work ATT3D [17]. Considering that the code of ATT3D is not publicly available, we retrain and evaluate our model on the dataset of ATT3D composed of 2,400 texts for a better comparison. Although ATT3D also aims for fast text-to-3D generation similar to this work, it requires per-prompt fine-tuning after each network inference, leading to lower efficiency. Moreover, with the techniques proposed in Section 3, our network is more effective than the model of ATT3D, which significantly improves the generation quality.

**Qualitative Comparison.** We compare our generated objects with those of ATT3D in Figure 13. The animals generated by ATT3D are blurry and lack essential details, and some described items in the prompts are not distinguishable.



Figure 13: Comparison with the concurrent work ATT3D. The text prompts are given in the last row. Our generated 3D objects contain more details and are more distinguishable with better interactions between animals and items.

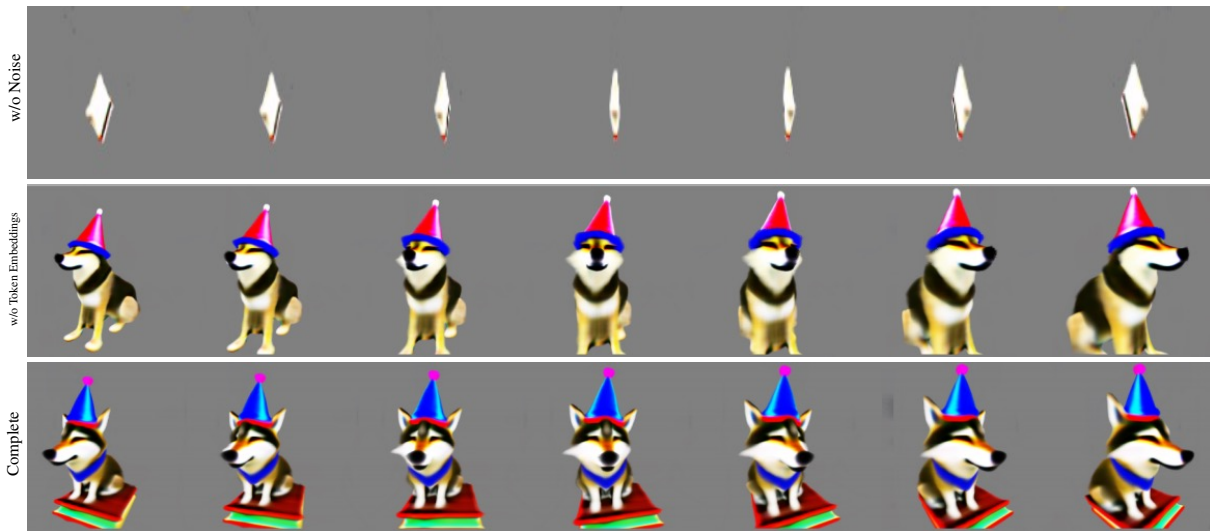


Figure 14: Effectiveness of the proposed style injection module. Top: without Gaussian noise; middle: without token embeddings; bottom: full model. The prompt is “a wolf sitting on books and wearing a tie and wearing a party hat”. The comparison shows that the incorporation of Gaussian noise prevents training collapse, and the token embeddings contribute to better text-3D consistency.

Moreover, the interactions between animals and their holding items could be disordered, for example, the erroneous orientations of the guitar and katana. In contrast, our *Instant3D* consistently produces sharp renderings and ensures plausible interactions between entities.

**Computation Costs.** We compare our computation cost with ATT3D by reporting Views-PP vs. CLIP-RP in Figure 12. As the code of ATT3D is not accessible to the public, we directly extract the reported numbers from the original paper [17]. Notably, our *Instant3D* requires fewer renderings per prompt during optimization, yet achieves superior text-3D alignment, underscoring its efficiency and ef-

fectiveness in high-quality text-to-3D generation.

**User Preference Study.** We also conduct user studies to compare ATT3D and our approach based on user preferences. We show users videos rendered from multiple views of objects generated by two methods for the same text prompt. We ask them to select the result that has better quality in realism and text-3D consistency. To enhance the reliability of our study and mitigate variance, each prompt is evaluated by at least 3 different users. As shown in Table 2, the results of our *Instant3D* are clearly preferred over those of the ATT3D in terms of both standards, highlighting the effectiveness of the proposed algorithm.

Table 2: User preference study for comparing our results against those of ATT3D in terms of image realism and text-3D consistency.

Method	ATT3D	<i>Instant3D</i>
Realism	8.68%	91.32%
Consistency	13.23%	86.77%

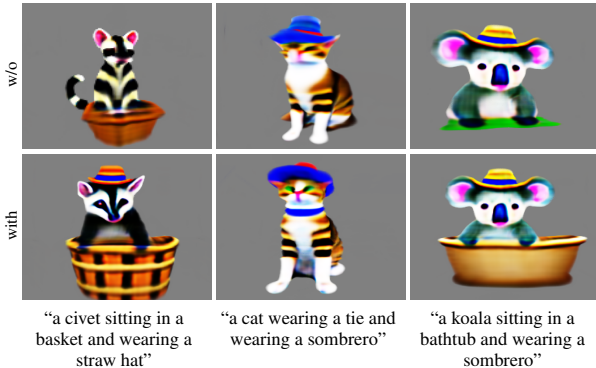


Figure 15: Effectiveness of the proposed token-to-plane transformation. Top: without token-to-plane transformation; bottom: full model.

#### 4.5. Ablation Study

We conduct extensive ablation studies on the Animals set to investigate the effectiveness of the key components in our network, including the style injection module, token-to-plane transformation, scaled-sigmoid function, and the adaptive Perp-Neg algorithm.

**Effectiveness of Style Injection.** To evaluate the importance of our style injection module in Figure 4, we evaluate two ablated versions: one without Gaussian noise and the other excluding token embeddings.

Comparing the top and bottom rows, it is evident that adding Gaussian noise is instrumental in circumventing the training collapse issue, which prevents generating null or meaningless outputs. The middle and bottom rows underscore the significance of token embeddings in the style injection module, which better inject textual conditions into the triplane generation process, leading to improved text-3D consistency under weak supervision signals.

**Effectiveness of Token-to-Plane Transformation.** To understand the effect of our token-to-plane transformation, we replace it with a learnable constant to feed into the decoder. As illustrated in Figure 15 (top), objects generated without token-to-plane transformation cannot be well controlled by the condition text prompts. For example, the expected hat is absent in the first column, and the bathtub is missing in the third column. In contrast, our full approach (bottom row) ensures all described items in the prompts are accurately

generated and interact in a plausible manner.

**Effectiveness of Scaled-Sigmoid.** In Section 3.3, we introduce a scaled-sigmoid function for NeRF albedo prediction to accelerate the training process. To verify this design, we provide a comparison between the scaled-sigmoid and the conventional sigmoid function. Their corresponding generation processes for the same prompt are shown in Figure 16. The numbers below images are the training iterations in terms of Views-PP. It is evident that the 3D generation driven by the standard sigmoid activation evolves much slower than that of the scaled-sigmoid. Notably, even with ten times training iterations of the scaled-sigmoid, the network with the conventional sigmoid function still does not achieve satisfactory convergence. The evolution process of the generated 3D object also shows that the scaled-sigmoid enables a more significant capability of our model in adjusting the output to match the text description.

**Effectiveness of Adaptive Perp-Neg.** As detailed in Section 3.4, we propose the adaptive Perp-Neg algorithm to address the Janus problem commonly encountered in text-to-3D. To understand the benefits of this algorithm, we provide a comparison against the original Perp-Neg algorithm where  $w_{\text{neg}}$  remains fixed throughout training. As shown in Figure 17 (top), it is not feasible to find a universally optimum value for all objects: the Janus problem is not fully resolved in the first column (three feet for the teddy bear), which indicates the  $w_{\text{neg}}$  is too small; but for the other two columns, the Janus problem has been overly punished, evidenced by flat faces, which indicates the  $w_{\text{neg}}$  is too large. In Figure 17 (bottom), as our adaptive Perp-Neg can dynamically adjust  $w_{\text{neg}}$  for each object according to the severity of the Janus problem, it effectively overcomes the above challenge and produces higher-quality results.

## 5. Conclusion

In this paper, we demonstrate the feasibility of fast text-to-3D generation with a one-pass feedforward network. To overcome the learning difficulties brought by weak supervision from SDS loss, we integrate three condition mechanisms, *i.e.*, cross-attention, style injection, and token-to-plane transformation, to better embed text prompts into a decoder network. We also present a scaled-sigmoid function for albedo activation, which accelerates the optimization convergence by more than ten times. In addition, we propose an adaptive Perp-Neg algorithm, which effectively tackles the Janus problem in our new paradigm without introducing extra computation costs. Extensive experiments on three prompt sets show that our *Instant3D* is able to generate faithful 3D objects for novel prompts in less than one second. Moreover, our approach shows much better optimization efficiency. We expect this work to inspire further explorations in fast text-to-3D generation.

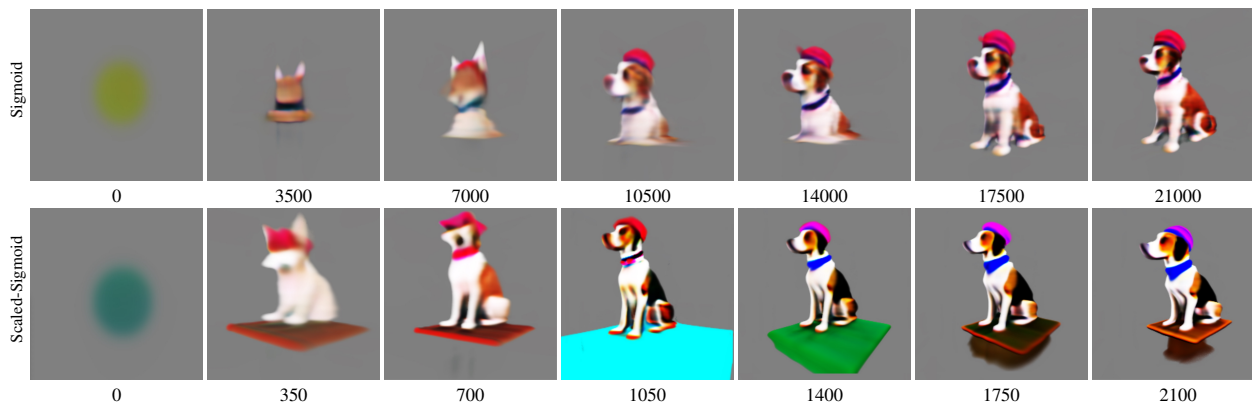


Figure 16: Evolution process of the generated objects with the conventional sigmoid activation (top) and the scaled-sigmoid activation (bottom) for albedo prediction. The number below each image is the corresponding training iteration in terms of Views-PP. The prompt is “a dog sitting on a table and wearing a tie and wearing a beanie”. The scaled-sigmoid function significantly accelerates the training convergence and enables better capability in text-3D alignment.

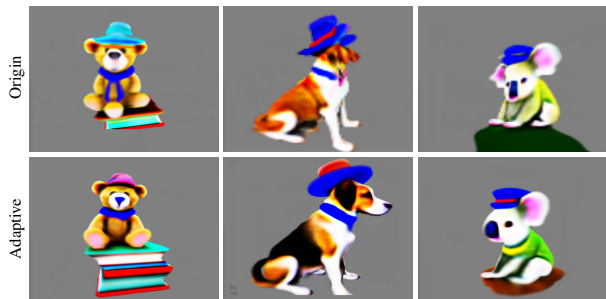


Figure 17: Comparison of the generated objects by using the original Perp-Neg algorithm (top) and our adaptive variant (bottom). In the top row, the teddy bear has three feet, while the dog and koala already display severe flat faces. This suggests that the original algorithm can not simultaneously address Janus problem for multiple objects. In contrast, our adaptive algorithm adjusts the concept negation scales of various objects during the generation process and significantly overcomes the above challenge.

## Acknowledgement

Ming Li is funded by the ISEP-IDS PhD scholarship in NUS. Xiangyu Xu acknowledges the computational resources provided by the HPC platform of Xi’an Jiaotong University.

## References

[1] Mohammadreza Armandpour, Huangjie Zheng, Ali Sadeghian, Amir Sadeghian, and Mingyuan Zhou. Re-imagine the negative prompt algorithm: Transform 2d diffusion into 3d, alleviate janus problem and beyond. *arXiv preprint arXiv:2304.04968*, 2023. 2, 6

[2] Tom Brown, Benjamin Mann, Nick Ryder, Melanie Subbiah, Jared D Kaplan, Prafulla Dhariwal, Arvind Neelakantan, Pranav Shyam, Girish Sastry, Amanda Askell, et al. Language models are few-shot learners. *Advances in neural information processing systems*, 33:1877–1901, 2020. 8

[3] Eric R Chan, Connor Z Lin, Matthew A Chan, Koki Nagano, Boxiao Pan, Shalini De Mello, Orazio Gallo, Leonidas J Guibas, Jonathan Tremblay, Sameh Khamis, et al. Efficient geometry-aware 3d generative adversarial networks. In *Proceedings of the IEEE/CVF Conference on Computer Vision and Pattern Recognition*, pages 16123–16133, 2022. 2, 4

[4] Ming Ding, Zhuoyi Yang, Wenyi Hong, Wendi Zheng, Chang Zhou, Da Yin, Junyang Lin, Xu Zou, Zhou Shao, Hongxia Yang, et al. Cogview: Mastering text-to-image generation via transformers. *Advances in Neural Information Processing Systems*, 34:19822–19835, 2021. 2

[5] Patrick Esser, Robin Rombach, and Bjorn Ommer. Taming transformers for high-resolution image synthesis. In *Proceedings of the IEEE/CVF Conference on Computer Vision and Pattern Recognition (CVPR)*, pages 12873–12883, June 2021. 2

[6] Ian Goodfellow, Jean Pouget-Abadie, Mehdi Mirza, Bing Xu, David Warde-Farley, Sherjil Ozair, Aaron Courville, and Yoshua Bengio. Generative adversarial networks. *Communications of the ACM*, 63(11):139–144, 2020. 2

[7] Jonathan Ho, Ajay Jain, and Pieter Abbeel. Denoising diffusion probabilistic models. *Advances in Neural Information Processing Systems*, 33:6840–6851, 2020. 2

[8] Jonathan Ho and Tim Salimans. Classifier-free diffusion guidance. *arXiv preprint arXiv:2207.12598*, 2022. 3

[9] Ajay Jain, Ben Mildenhall, Jonathan T. Barron, Pieter Abbeel, and Ben Poole. Zero-shot text-guided object generation with dream fields. In *Proceedings of the IEEE/CVF Conference on Computer Vision and Pattern Recognition (CVPR)*, pages 867–876, June 2022. 1, 3

- [10] Tero Karras, Miika Aittala, Samuli Laine, Erik Härkönen, Janne Hellsten, Jaakko Lehtinen, and Timo Aila. Alias-free generative adversarial networks. In *NeurIPS*, 2021. 5
- [11] Tero Karras, Samuli Laine, and Timo Aila. A style-based generator architecture for generative adversarial networks. In *Proceedings of the IEEE/CVF conference on computer vision and pattern recognition*, pages 4401–4410, 2019. 4, 5
- [12] Tero Karras, Samuli Laine, Miika Aittala, Janne Hellsten, Jaakko Lehtinen, and Timo Aila. Analyzing and improving the image quality of StyleGAN. In *CVPR*, 2020. 5
- [13] Nasir Mohammad Khalid, Tianhao Xie, Eugene Belilovsky, and Popa Tiberiu. Clip-mesh: Generating textured meshes from text using pretrained image-text models. *SIGGRAPH Asia 2022 Conference Papers*, December 2022. 3
- [14] Diederik P Kingma and Jimmy Ba. Adam: A method for stochastic optimization. *arXiv preprint arXiv:1412.6980*, 2014. 8
- [15] Han-Hung Lee and Angel X Chang. Understanding pure clip guidance for voxel grid nerf models. *arXiv preprint arXiv:2209.15172*, 2022. 3
- [16] Zhengzhe Liu, Peng Dai, Ruihui Li, Xiaojuan Qi, and Chi-Wing Fu. Iss: Image as stetting stone for text-guided 3d shape generation. *arXiv preprint arXiv:2209.04145*, 2022. 3
- [17] Jonathan Lorraine, Kevin Xie, Xiaohui Zeng, Chen-Hsuan Lin, Towaki Takikawa, Nicholas Sharp, Tsung-Yi Lin, Ming-Yu Liu, Sanja Fidler, and James Lucas. Att3d: Amortized text-to-3d object synthesis. *arXiv preprint arXiv:2306.07349*, 2023. 3, 11, 12
- [18] Gal Metzer, Elad Richardson, Or Patashnik, Raja Giryes, and Daniel Cohen-Or. Latent-nerf for shape-guided generation of 3d shapes and textures. In *Proceedings of the IEEE/CVF Conference on Computer Vision and Pattern Recognition*, 2023. 1, 3, 4, 6, 8, 9
- [19] Ben Mildenhall, Pratul P. Srinivasan, Matthew Tancik, Jonathan T. Barron, Ravi Ramamoorthi, and Ren Ng. Nerf: Representing scenes as neural radiance fields for view synthesis. In *ECCV*, 2020. 1, 3
- [20] Thomas Müller, Alex Evans, Christoph Schied, and Alexander Keller. Instant neural graphics primitives with a multiresolution hash encoding. *ACM Transactions on Graphics (ToG)*, 41(4):1–15, 2022. 3
- [21] Alex Nichol, Prafulla Dhariwal, Aditya Ramesh, Pranav Shyam, Pamela Mishkin, Bob McGrew, Ilya Sutskever, and Mark Chen. Glide: Towards photorealistic image generation and editing with text-guided diffusion models. *arXiv preprint arXiv:2112.10741*, 2021. 2
- [22] Alex Nichol, Heewoo Jun, Prafulla Dhariwal, Pamela Mishkin, and Mark Chen. Point-e: A system for generating 3d point clouds from complex prompts. *arXiv preprint arXiv:2212.08751*, 2022. 2, 8, 9
- [23] Ben Poole, Ajay Jain, Jonathan T Barron, and Ben Mildenhall. Dreamfusion: Text-to-3d using 2d diffusion. *arXiv preprint arXiv:2209.14988*, 2022. 1, 2, 3, 4, 8, 9
- [24] Tingting Qiao, Jing Zhang, Duanqing Xu, and Dacheng Tao. Mirrorgan: Learning text-to-image generation by redescription. In *Proceedings of the IEEE/CVF Conference on Computer Vision and Pattern Recognition (CVPR)*, June 2019. 2
- [25] Alec Radford, Jong Wook Kim, Chris Hallacy, Aditya Ramesh, Gabriel Goh, Sandhini Agarwal, Girish Sastry, Amanda Askell, Pamela Mishkin, Jack Clark, et al. Learning transferable visual models from natural language supervision. In *International Conference on Machine Learning*, pages 8748–8763. PMLR, 2021. 2, 5
- [26] Aditya Ramesh, Prafulla Dhariwal, Alex Nichol, Casey Chu, and Mark Chen. Hierarchical text-conditional image generation with clip latents. *arXiv preprint arXiv:2204.06125*, 2022. 2
- [27] Aditya Ramesh, Mikhail Pavlov, Gabriel Goh, Scott Gray, Chelsea Voss, Alec Radford, Mark Chen, and Ilya Sutskever. Zero-shot text-to-image generation. In *International Conference on Machine Learning*, pages 8821–8831. PMLR, 2021. 2
- [28] Scott Reed, Zeynep Akata, Xinchun Yan, Lajanugen Logeswaran, Bernt Schiele, and Honglak Lee. Generative adversarial text to image synthesis. In *International conference on machine learning*, pages 1060–1069. PMLR, 2016. 2
- [29] Robin Rombach, Andreas Blattmann, Dominik Lorenz, Patrick Esser, and Björn Ommer. High-resolution image synthesis with latent diffusion models. In *Proceedings of the IEEE/CVF Conference on Computer Vision and Pattern Recognition*, pages 10684–10695, 2022. 2, 3, 5, 8
- [30] Shulan Ruan, Yong Zhang, Kun Zhang, Yanbo Fan, Fan Tang, Qi Liu, and Enhong Chen. Dae-gan: Dynamic aspect-aware gan for text-to-image synthesis. In *Proceedings of the IEEE/CVF International Conference on Computer Vision (ICCV)*, pages 13960–13969, October 2021. 2
- [31] Chitwan Saharia, William Chan, Saurabh Saxena, Lala Li, Jay Whang, Emily Denton, Seyed Kamyar Seyed Ghasemipour, Burcu Karagol Ayan, S Sara Mahdavi, Rapha Gontijo Lopes, et al. Photorealistic text-to-image diffusion models with deep language understanding. *arXiv preprint arXiv:2205.11487*, 2022. 2
- [32] Aditya Sanghi, Hang Chu, Joseph G. Lambourne, Ye Wang, Chin-Yi Cheng, Marco Fumero, and Kamal Rahimi Malekshah. Clip-forge: Towards zero-shot text-to-shape generation. In *Proceedings of the IEEE/CVF Conference on Computer Vision and Pattern Recognition (CVPR)*, pages 18603–18613, June 2022. 3
- [33] Christoph Schuhmann, Romain Beaumont, Richard Vencu, Cade Gordon, Ross Wightman, Mehdi Cherti, Theo Coombes, Aarush Katta, Clayton Mullis, Mitchell Wortsman, et al. Laion-5b: An open large-scale dataset for training next generation image-text models. *arXiv preprint arXiv:2210.08402*, 2022. 2
- [34] Christoph Schuhmann, Richard Vencu, Romain Beaumont, Robert Kaczmarczyk, Clayton Mullis, Aarush Katta, Theo Coombes, Jenia Jitsev, and Aran Komatsuzaki. Laion-400m: Open dataset of clip-filtered 400 million image-text pairs. *arXiv preprint arXiv:2111.02114*, 2021. 2
- [35] Jiaming Song, Chenlin Meng, and Stefano Ermon. Denoising diffusion implicit models. *arXiv preprint arXiv:2010.02502*, 2020. 2
- [36] Cheng Sun, Min Sun, and Hwann-Tzong Chen. Direct voxel grid optimization: Super-fast convergence for radiance fields

- reconstruction. In *Proceedings of the IEEE/CVF Conference on Computer Vision and Pattern Recognition (CVPR)*, pages 5459–5469, June 2022. 3
- [37] Hongchen Tan, Xiuping Liu, Xin Li, Yi Zhang, and Baocai Yin. Semantics-enhanced adversarial nets for text-to-image synthesis. In *Proceedings of the IEEE/CVF International Conference on Computer Vision (ICCV)*, October 2019. 2
- [38] Christina Tsalicoglou, Fabian Manhardt, Alessio Tonioni, Michael Niemeyer, and Federico Tombari. Textmesh: Generation of realistic 3d meshes from text prompts. *arXiv preprint arXiv:2304.12439*, 2023. 8, 9
- [39] Ashish Vaswani, Noam Shazeer, Niki Parmar, Jakob Uszkoreit, Llion Jones, Aidan N Gomez, Łukasz Kaiser, and Illia Polosukhin. Attention is all you need. *Advances in neural information processing systems*, 30, 2017. 5
- [40] Haochen Wang, Xiaodan Du, Jiahao Li, Raymond A Yeh, and Greg Shakhnarovich. Score jacobian chaining: Lifting pretrained 2d diffusion models for 3d generation. *arXiv preprint arXiv:2212.00774*, 2022. 4
- [41] Haochen Wang, Xiaodan Du, Jiahao Li, Raymond A Yeh, and Greg Shakhnarovich. Score jacobian chaining: Lifting pretrained 2d diffusion models for 3d generation. In *Proceedings of the IEEE/CVF Conference on Computer Vision and Pattern Recognition*, pages 12619–12629, 2023. 3, 8, 9
- [42] Zihao Wang, Wei Liu, Qian He, Xinglong Wu, and Zili Yi. Clip-gen: Language-free training of a text-to-image generator with clip. *arXiv preprint arXiv:2203.00386*, 2022. 2, 4, 5, 7
- [43] Zhengyi Wang, Cheng Lu, Yikai Wang, Fan Bao, Chongxuan Li, Hang Su, and Jun Zhu. Prolificdreamer: High-fidelity and diverse text-to-3d generation with variational score distillation. *arXiv preprint arXiv:2305.16213*, 2023. 1, 2, 3, 8, 9
- [44] Tao Xu, Pengchuan Zhang, Qiuyuan Huang, Han Zhang, Zhe Gan, Xiaolei Huang, and Xiaodong He. Attngan: Fine-grained text to image generation with attentional generative adversarial networks. In *Proceedings of the IEEE Conference on Computer Vision and Pattern Recognition (CVPR)*, June 2018. 2
- [45] Han Yi, Zhedong Zheng, Xiangyu Xu, and Tat-seng Chua. Progressive text-to-3d generation for automatic 3d prototyping. *arXiv preprint arXiv:2309.14600*, 2023. 3
- [46] Han Zhang, Tao Xu, Hongsheng Li, Shaoting Zhang, Xiaogang Wang, Xiaolei Huang, and Dimitris N. Metaxas. Stackgan: Text to photo-realistic image synthesis with stacked generative adversarial networks. In *Proceedings of the IEEE International Conference on Computer Vision (ICCV)*, Oct 2017. 2

# Instant3D: Instant Text-to-3D Generation

## APPENDIX

### 1. Daily Life Set

As stated in the main paper, our Daily Life prompt set is collected from ChatGPT, containing more than 17,000 prompts. The dataset is available at <https://drive.google.com/file/d/1-5GP4H2QJSPwIuUIfiEBjzPI7DwG9LOX/view?usp=sharing>.

### 2. Network Architecture

Our decoder network takes the output of the token-to-plane transformation as input, which has a resolution of  $8 \times 8$ . The decoder contains five stages: each of the first three stages consists of ten alternate attention and convolution blocks, while the last two stages only have convolution blocks. A  $\times 2$ -upsampling interpolation layer is applied after each stage, resulting in a triplane output with a resolution of  $256 \times 256$ .

**Attention Block.** The attention block is shown in Figure 1, which enables inner information interaction by multi-head self-attention and text-3D information interchange through multi-head cross-attention.

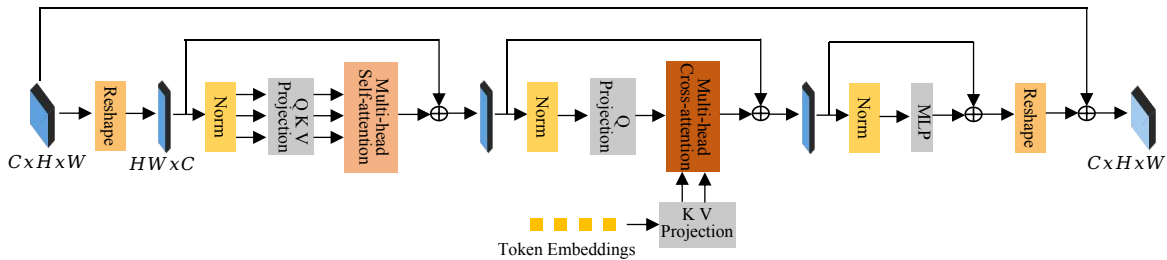


Figure 1: Illustration of the attention block, which mainly contains a self-attention mechanism for inner-feature map information interaction and a cross-attention mechanism for text-3D information interchange.

**Convolution Block.** The convolution block is illustrated in Figure 2, which uses Adaptive Instance Normalization (AdaIN) to absorb the style information from the style injection module. Convolution layers are used in this block to introduce spatial inductive bias.

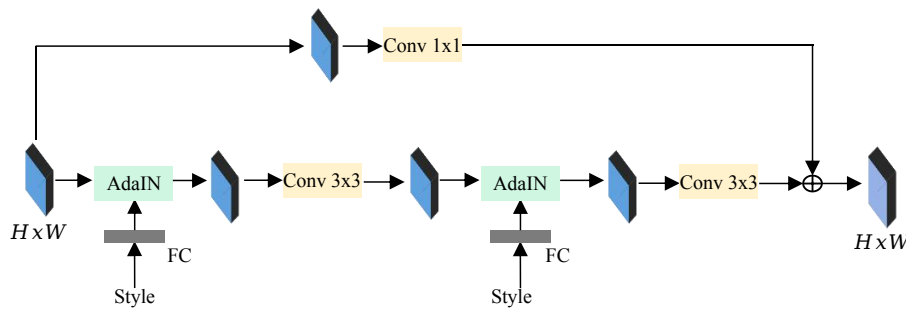


Figure 2: Illustration of the convolution block, which employs AdaIN to incorporate the output of the style injection module into the triplane generation.

### 3. More Visualization Results

We show more objects generated by our *Instant3D* trained on the Animals set (Figure 3), Portraits set (Figure 4), and Daily Life set (Figure 5). The results demonstrate that our *Instant3D* successfully generates faithful 3D objects for new prompts. Additionally, we also provide a video of our generated objects by rendering 120 images from a series of evenly distributed azimuth angles, showing our high-quality geometry. The video is available at <https://drive.google.com/file/d/1QdO5qtUrKA0WChAl6N-0g1FHs4M1LgBx/view?usp=sharing>.



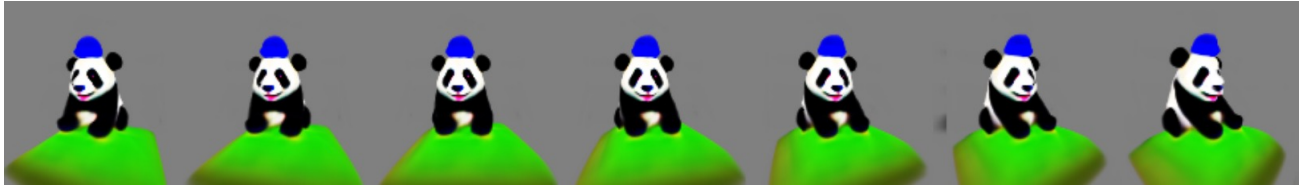
(a) “a dog sitting on the lawn and wearing a tie and wearing a sombrero”



(b) “a koala sitting on books and wearing a cape and wearing a baseball cap”



(c) “a rabbit sitting on a stone and wearing a beret”



(d) “a panda sitting on the lawn and wearing a beanie”



(e) “a rabbit sitting in a basket and wearing a tie”



(f) “a dog sitting on a stone and wearing a tie and wearing a beanie”

Figure 3: More results on the Animals set, which are inferred directly by our *Instant3D* for novel prompts. We visualize continuous view images rendered around the front direction of each object to show the cross-view consistency.



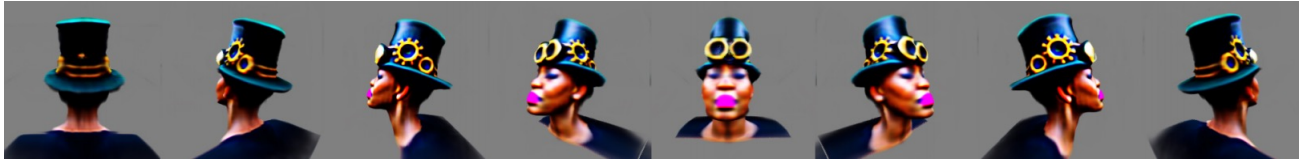
(a) “an elderly woman wearing a Santa hat is looking ahead with a very serious expression”



(b) “a girl wearing a Santa hat is angry”



(c) “Obama wearing a peaked cap is talking”



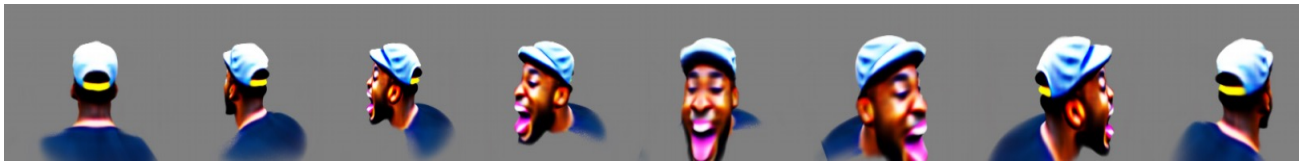
(d) “a black woman wearing a steampunk hat is feeling sad”



(e) “a boy wearing a peaked cap is shouting”



(f) “an elderly man wearing a crown is opening mouth wide in shock”



(g) “a black man wearing a peaked cap is laughing”

Figure 4: More results on the Portraits set. The prompts describe various figures wearing different hats and expressing different emotions. We visualize continuous view images rendered from each object.

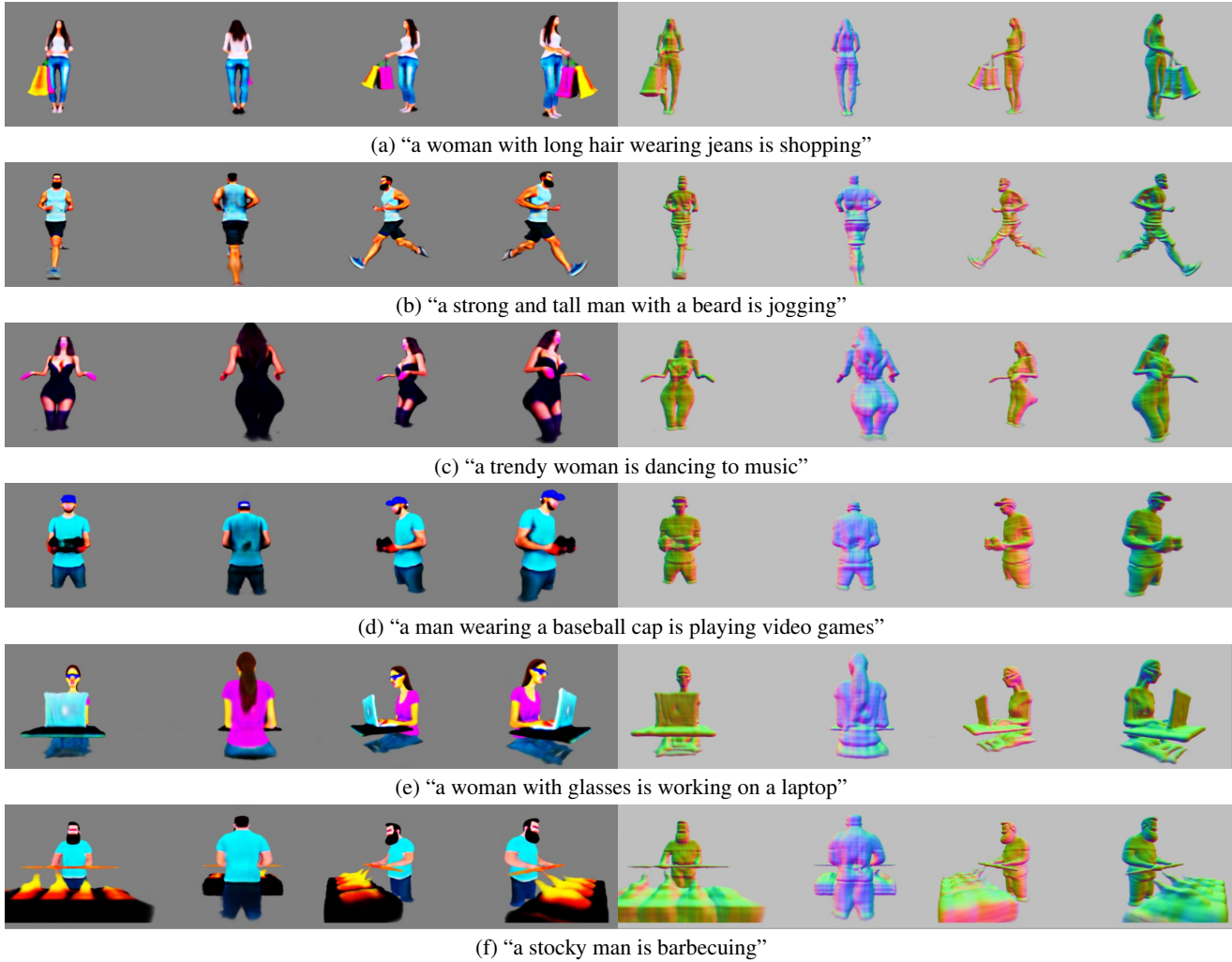


Figure 5: More generated objects for new testing prompts by our *Instant3D* trained on the Daily Life set. For each prompt, four view images and their normal images are shown. Our framework is able to generate complex and diverse objects for new prompts with high-quality geometric details.